Journal of Power Sources 195 (2010) 2961–2968

Contents lists available at ScienceDirect

Journal of Power Sources

journal homepage: www.elsevier.com/locate/jpowsour

Thermal modeling of a cylindrical $LiFePO_4$/graphite lithium-ion battery

Christophe Forgez[a,*], Dinh Vinh Do[a], Guy Friedrich[a], Mathieu Morcrette[b], Charles Delacourt[b]

[a] Université de Technologie de Compiègne, EA 1006, Laboratoire d'Electromécanique de Compiègne, BP 20529, 60205 Compiègne Cedex, France
[b] Laboratoire de Réactivité et de Chimie des Solides, UMR 6007, Université de Picardie Jules Verne, 33 Rue Saint Leu, 80039 Amiens, France

ARTICLE INFO

Article history:
Received 29 July 2009
Received in revised form 1 October 2009
Accepted 20 October 2009
Available online 13 November 2009

Keywords:
Li-ion battery
Thermal modeling
Temperature
Heat source

ABSTRACT

A lumped-parameter thermal model of a cylindrical $LiFePO_4$/graphite lithium-ion battery is developed. Heat transfer coefficients and heat capacity are determined from simultaneous measurements of the surface temperature and the internal temperature of the battery while applying 2 Hz current pulses of different magnitudes. For internal temperature measurements, a thermocouple is introduced into the battery under inert atmosphere. Heat transfer coefficients (thermal resistances in the model) inside and outside the battery are obtained from thermal steady state temperature measurements, whereas the heat capacity (thermal capacitance in the model) is determined from the transient part. The accuracy of the estimation of internal temperature from surface temperature measurements using the model is validated on current-pulse experiments and a complete charge/discharge of the battery and is within 1.5 °C. Furthermore, the model allows for simulating the internal temperature directly from the measured current and voltage of the battery. The model is simple enough to be implemented in battery management systems for electric vehicles.

1. Introduction

Most of the models used in battery management systems (BMS) and state of charge (SOC) or state of health (SOH) observers consist in lumped-parameter equivalent electric circuits that are to some degree in relation with the physical phenomena within the battery, such as charge transfer, diffusion, and double layer effects [1]. Generally, values of model parameters are obtained using electrochemical impedance spectroscopy (EIS) under various conditions of state of charge, state of health, and temperature. However, under regular operating conditions, the internal battery temperature departs significantly from that measured at the surface, hence the set of input parameters determined at a given temperature using low-current methods like EIS is no longer appropriate. Therefore, having a thermal model able to estimate the internal temperature of the battery under operation can help improving the accuracy of the model used in the BMS.

Several papers deal with thermal modeling of battery. In most of them, a thermal model is coupled with an electrochemical model so as to simulate the temperature profile of a battery under different operating conditions, geometries or cooling rate [2,3]. Such coupled models can also be used to explore pulse power limitations in order to prevent thermal runaway or to design heat dissipation systems [3–5]. Three-dimensional thermal models have also been investigated in order to provide a better insight about the behavior of cells under abuse conditions [6]. Such models are well-suited for the battery design purpose, but are not compatible with the low computational resources of micro-controllers used in BMS.

This paper presents a simplified thermal model able to estimate the internal temperature of the battery (assumed uniform) from surface temperature measurements, which is straightforward to implement in a low-cost micro-controller while enabling an improvement of the accuracy of the electrochemical model used in the BMS. The input parameters of the thermal model (heat transfer coefficients and heat capacity) are determined from transient experiments for which the battery temperature is raised using current pulses as the heat source instead of an external heating system as reported previously [7]. The internal temperature in the center of the cell is monitored by means of a thermocouple inserted into the cell and is used for parameter determination and model validation purpose. The model validation is restricted to regular temperature conditions (<60 °C), with natural-convection heat dissipation. Beside, the cell temperature coefficient, used for evaluation of the heat source term, is determined from open-circuit potential measurements at various temperatures and states of charge, and the enthalpy potential is derived.

After Section 2 where the experimental device is detailed, Section 3 presents the model development together with the assumptions that were used for simplification purpose. The way the input parameters of the thermal model were determined is detailed in Section 4. Finally, the model accuracy is assessed under various operating conditions in Section 5.

* Corresponding author.
E-mail address: christophe.forgez@utc.fr (C. Forgez).

0378-7753/$ – see front matter © 2009 Elsevier B.V. All rights reserved.
doi:10.1016/j.jpowsour.2009.10.105

Nomenclature

List of symbols

A, B, C	constants used in the fits
c_j	concentration of species j (mol m^{-3})
C_p	heat capacity (J K^{-1})
F	Faraday's constant (96,487 C mol^{-1})
h_{in}	heat transfer coefficient inside the battery (W K^{-1})
h_{out}	heat transfer coefficient outside the battery (W K^{-1})
$\bar{H}_j$	partial molar enthalpy of species j (J mol^{-1})
I	current (A)
n	number of electrons exchanged
q_n	heat flux transferred to the outside of the battery (W)
$\dot{Q}$	rate of heat generated or consumed (W)
r_i	rate of a chemical reaction i (mol s^{-1})
R_{in}	heat transfer resistance inside the cell (K W^{-1})
R_{out}	heat transfer resistance outside the cell (K W^{-1})
t	time (s)
T	temperature (K)
T_{amb}	bulk temperature of air (K)
T_{in}	internal temperature of the battery (K)
T_{surf}	surface temperature of the battery (K)
U	equilibrium potential of the cell (V)
U_H	enthalpy potential of the cell (V)
v	volume (m^3)
V	cell voltage (V)
ΔH_i	variation of the enthalpy of a chemical reaction i (J mol^{-1})
ΔS	variation of entropy of the cell reaction (J K^{-1} mol^{-1})
τ	constant used in a fit

superscript

avg	property evaluated at the volume-averaged concentration
∞	variable at steady state

2. Experimental

A $LiFePO_4$/graphite lithium-ion battery (26650 cyclindrical cell) was equipped with two T-type thermocouples (TC Direct, France): one on the surface and another one inserted into the battery (Fig. 1a) after it was discharged and drilled in the center of the positive electrode side. The thermocouple for internal temperature measurement was an insulated thermocouple (321 stainless steel sheath) of 1 mm external diameter. This diameter is chosen to be as close as possible to the diameter of the central hole in the battery roll to get a good thermal contact. The thermocouple for surface temperature measurement is a non-insulated one. A resin was used to ensure a good seal between the inner thermocouple and the battery casing. The overall process was carried out inside a argon-filled glove-box so as to ensure an inert atmosphere.

2.1. Measurements under current pulses

During experiments, the battery was kept away from external heat sources, and was placed in air with an ambient temperature of 22 °C. In order to raise the temperature of the battery, symmetrical and periodic current pulses with 2 Hz frequency and of different magnitudes (±10, ±15, and ±20 A) were applied to the battery using a power amplifier (VMP3 Biologic, Claix, France, Fig. 1b). The pulses are symmetrical in order to hold the battery at an average state of charge (50%) over time. This SOC value was chosen since this is an average value used in many applications (this is for operating

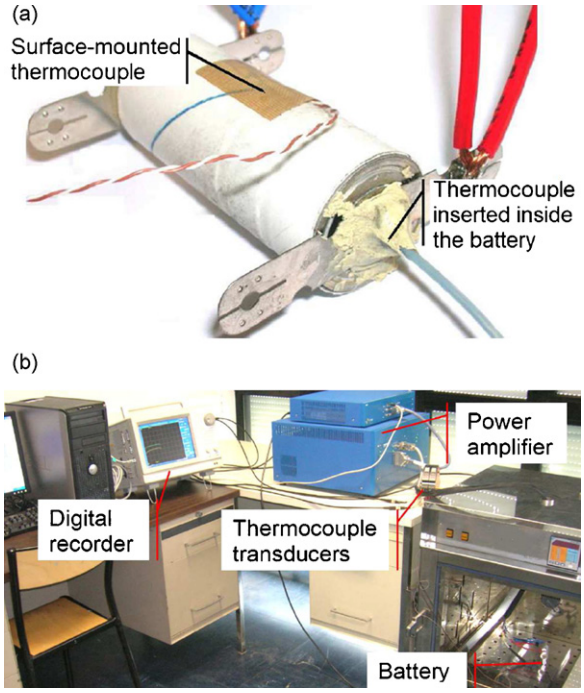

Fig. 1. (a) Battery with inserted and surface mounted thermocouples and (b) experimental device

conditions around that SOC that the battery exhibits the maximum charge/discharge power). Of course, one could reproduce the same tests at other average SOCs in order to get the SOC-dependence of the model parameters (C_p and R_{in}). A 2 Hz frequency was selected from an analysis of the impedance spectra of the battery, which shows that this frequency is intermediate between the low frequency of the interfacial part and the high frequency of the diffusion part. Output voltages from both thermocouples were recorded using a digital scope (Yokogawa DL716, Fig. 1b) and further converted to temperatures. Fig. 2 displays the experimental surface and internal temperature data measurements when current pulses of different magnitudes (±10, ±15, and ±20 A) are applied during one hour (0–3600 s in the plots, Fig. 2), after which the current is turned off to allow for temperature relaxation. From the Fig. 2, it is seen that a thermal steady state has been reached after around an hour under current pulses. Furthermore, whatever the magnitude of the current pulses, the temperature dynamics seem to be similar, with a non-zero slope at initial time indicative of a first-order behavior.

2.2. Measurements under open-circuit potential (OCP)

OCP measurements were carried out for cell temperatures ranging from 6 to 36 ° C at different SOCs using a VMP3 potentiostat (Biologic, Claix, France) and a programmable climatic chamber (Binder KB53, Germany). The SOC was changed using a C/20 current at 25 ° C and the battery was subsequently allowed to relax for 5 h at the same temperature, after which the thermal cycle (16 °C, 3 h; 6 °C, 3 h; 21 °C, 3 h; 36 °C, 3 h; 26 °C, 3 h) was applied.

3. Thermal model

3.1. Energy balance

The equation for energy balance inside the cell reads

$$C_p \frac{\partial T_{in}}{\partial t} = -q_n + \dot{Q}, \quad (1)$$

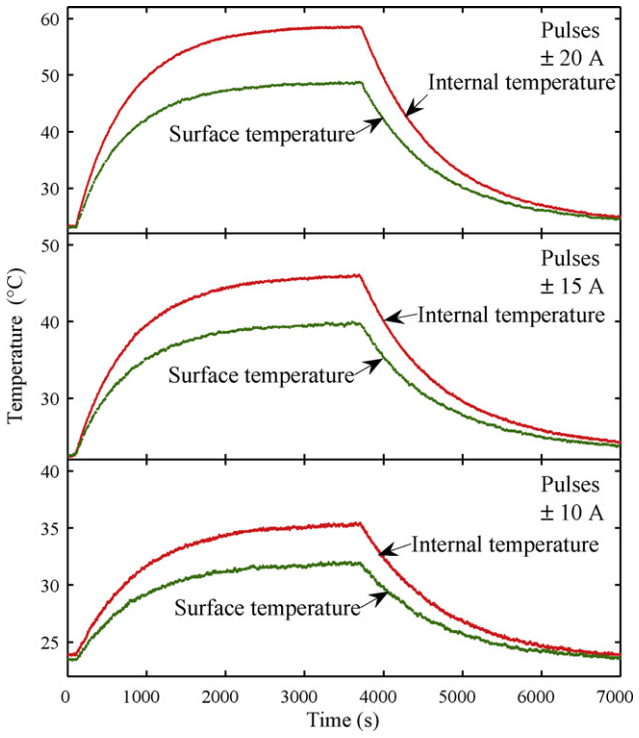

Fig. 2. Temperature measurements inside and on the surface for current pulses of magnitude ±10, ±15, and ±20 A.

where C_p is the heat capacity, T_{in} the bulk (or internal) temperature of the battery, t the time, $\dot{Q}$ the rate of heat generated (>0) or consumed (<0), and q_n is the heat flux transferred to the outside of the battery. q_n is related to the temperature difference between the bulk and the surface by means of a heat transfer coefficient. Applying such a relationship inside and outside the battery, the flux conservation equation reads

$$q_n = h_{in}(T_{in} - T_{surf}) = -h_{out}(T_{amb} - T_{surf}). \quad (2)$$

In Eq. (2), h_{in} and h_{out} are the heat transfer coefficients inside and outside the battery, respectively, T_{surf} is the surface temperature of the battery, and T_{amb} is the bulk temperature of air, far enough from the surface of the battery. Note that the heat transfer coefficients encompass different heat transport modes such as conduction, convection, and radiation. The predominant transport mode within the battery is the conduction, while convection and radiation are the more likely modes in the surrounding air. The readers are invited to consult specific literature for more details [8].

In the approach developed throughout this paper, the thermal model is described using equivalent electric circuits, where capacitances are used for heat capacities and resistances are used for the inverse of heat transfer coefficients. Now let us detail the mathematical expression for the rate of heat generated or consumed in the battery.

3.2. Heat source in the cell

An expression for the heat source in a lithium-ion battery was derived by Thomas and Newman [9]. It reads

$$\dot{Q} = I(V - U^{\text{avg}}) + IT\frac{\partial U^{\text{avg}}}{\partial T} - \sum_i \Delta H_i^{\text{avg}} r_i - \int \sum_j \left(\bar{H}_j - \bar{H}_j^{\text{avg}}\right)\frac{\partial c_j}{\partial t}\,dv, \quad (3)$$

with $\dot{Q}$ the rate of heat generated or consumed, V the cell voltage, U the equilibrium potential, I the current (>0 on charge), T the temperature, ΔH_i the variation of enthalpy of a chemical reaction i, r_i the rate of reaction i, $\bar{H}_j$ the partial molar enthalpy of species j, c_j its concentration, t the time, and v the volume. The superscript 'avg' indicates that the properties are evaluated at the volume-averaged concentration. The first term on the right is the heat generated from resistive dissipation, and is always positive. The second term is the reversible entropic heat (we recall that $\Delta S/nF = \partial U/\partial T$, with ΔS the entropy change of the cell reaction, n the number of electrons exchanged and F Faraday's constant.). This term can be either positive or negative. The third term represents the heat produced or consumed by any chemical reaction that may occur in the cell, and is either positive or negative as well. In the cylindrical cell under consideration in this study, side reactions accounting for aging are assumed to be slow enough to be neglected, so is also the third term in Eq. (3). Finally, the last term accounts for the heat of mixing, which is due to the formation and relaxation of concentration gradients within the cell. Such gradients may develop across the solid active materials of the porous electrodes and across the electrolyte (in the electrodes and the separator), as well as radially within the active material particles and within the pores of the electrode filled with electrolyte. Heat mixing terms can be either positive or negative. A general trend is that for electrochemical systems with good transport properties, concentration gradients are limited and heat of mixing can usually be ignored. Because the battery under consideration is designed for high power applications, it is thought to follow the above statement. Furthermore, because the positive electrode is a two-phase material, the two heat of mixing terms due to concentration gradients within the active material are zero. Although an insertion electrode material is used as the negative electrode, i.e., the graphite, the two heat of mixing terms within this active material are likely very small since the variations of the enthalpy potential U_H ($U_H = U - T\partial U/\partial T$) with lithium concentration are moderate [9,10]. This is also verified from the experimental measurements we performed and that are detailed in the next paragraph.

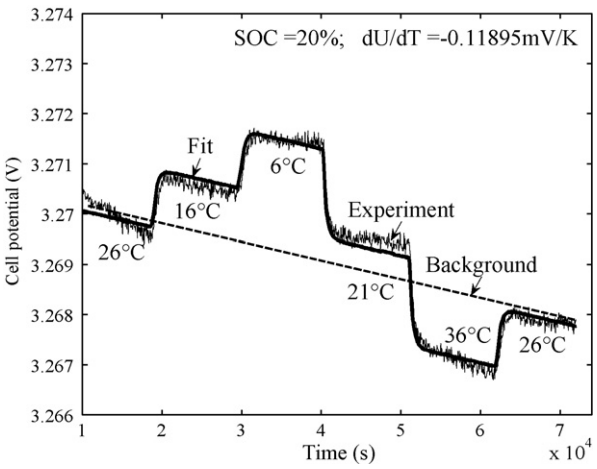

Fig. 3. Example of the voltage variation during the thermal cycle for SOC 20%.

The reversible heat source term (second term on the right hand side of Eq. (3)) is most often not negligible; it is of the same order of magnitude as the irreversible term [9]. We performed OCP experiments at various temperatures in order to determine the temperature coefficient and enthalpy potential as a function of the SOC. As emphasized by Thomas et al. [10,11], it is more convenient to vary the cell temperature for a given SOC rather than the reverse. Therefore, this method was utilized here. Fig. 3 provides an example of the voltage variation while the thermal cycle is applied. There is a slight drift of the cell voltage over time, which is not correlated with the temperature change, and which is ascribed to the cell

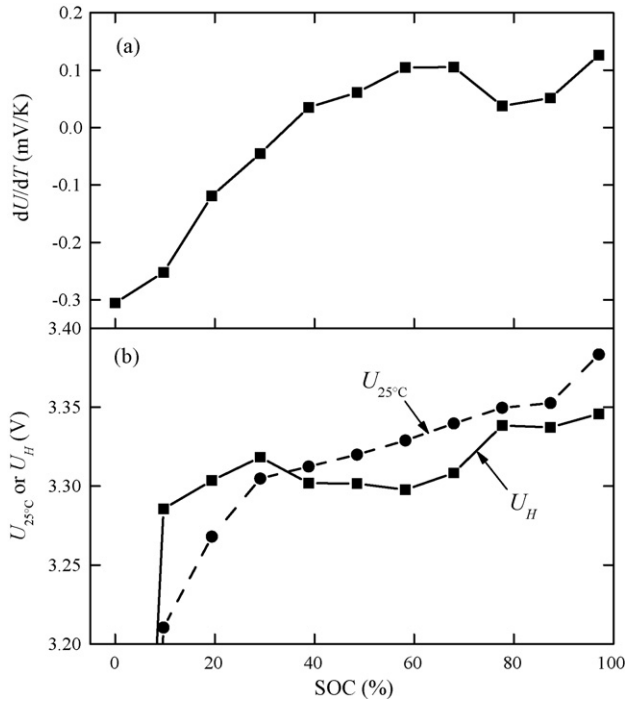

Fig. 4. (a) Temperature coefficient $\partial U/\partial T$ and (b) equilibrium potential at 25 °C $U_{25°C}$ and enthalpy potential U_H as a function of SOC.

relaxation following the previous SOC change. In order to extract the temperature coefficient from these data, the voltage was fit to a function $V(t, T) = A + BT + Ct$ with A, B, and C some constants, and B corresponding to the temperature coefficient $\partial U/\partial T$.

Fig. 4 presents the variation of $\partial U/\partial T$ with the SOC, together with that of the equilibrium potential U and the enthalpy potential U_H. The temperature coefficient is negative up to SOC 35%, and becomes positive for higher SOC values. It is interesting to compare U and U_H: while U is monotonic and increases with the SOC as expected, U_H is not. Furthermore, the dependence of $\partial U/\partial T$ and U_H with the SOC presents some similitudes with that of graphite/lithium cells [10,12], which is not surprising since in most of the composition ranges explored here, the positive electrode $LiFePO_4$ undergoes a two-phase process and therefore no variation of $\partial U/\partial T$ (and U_H) are expected. The fairly abrupt variation between SOC 70% and SOC 80% probably corresponds to the transition between the first and second stages of the graphite. This would indicate an excess of graphite over the positive electrode material, as it is frequently observed in commercial lithium-ion batteries.

Although the reversible heat source term cannot be neglected, for the current-pulse experiments used in this study, the cell temperature during a single period of current (0.5 s for parameters determination or 20 s for model validation) can be regarded as a constant, and therefore the average reversible heat source term over a period is almost zero. It is consequently discarded in the heat source term evaluation with the current pulses used in the following.

The irreversible source term (first term on the right hand side of Eq. (3)) is directly calculated for each test from the current and voltage values recorded every 10 ms. It is subsequently smoothed using a function of the type $I(V - U) = A + B\ \exp(-t/\tau)$, where A, B, and τ are refined by least square regression. The experimental and fitted curves are overlaid in Fig. 5.

3.3. Lumped model

As explained above, the energy balance (Eq. (1)) is represented using an equivalent electric circuit, where capacitors and resistors are used for accumulation terms and heat transfer phenomena, respectively, and a current source is used for the heat source term $\dot{Q}$. Equivalent circuits with different degrees of complexity may be chosen (Fig. 6). For instance, if the lateral surface temperature differs from that of the bases of the cylindrical battery, an equivalent circuit such as that of Fig. 6a would be used, in which heat fluxes inside and outside the battery are considered explicitly in axial and lateral directions. Furthermore, the different heat transport modes that may coexist can be visualized by a parallel association of resistors, as it is done for heat transport in the air surrounding the battery, for which convective and radiative effects are considered explicitely.

The main limitation of using such a detailed lumped model is that there are a lot of parameters to be determined, which usually requires additional experimental measurements. Since the goal of this work is to build a model that is able to get an estimate of the internal temperature of the battery from a simple measurement of the lateral surface temperature, simplifications to the equivalent circuit of Fig. 6a can be made. Under the assumption that the surface temperature of the battery is uniform (i.e. the surface temperature of the terminals is close to the lateral temperature), the

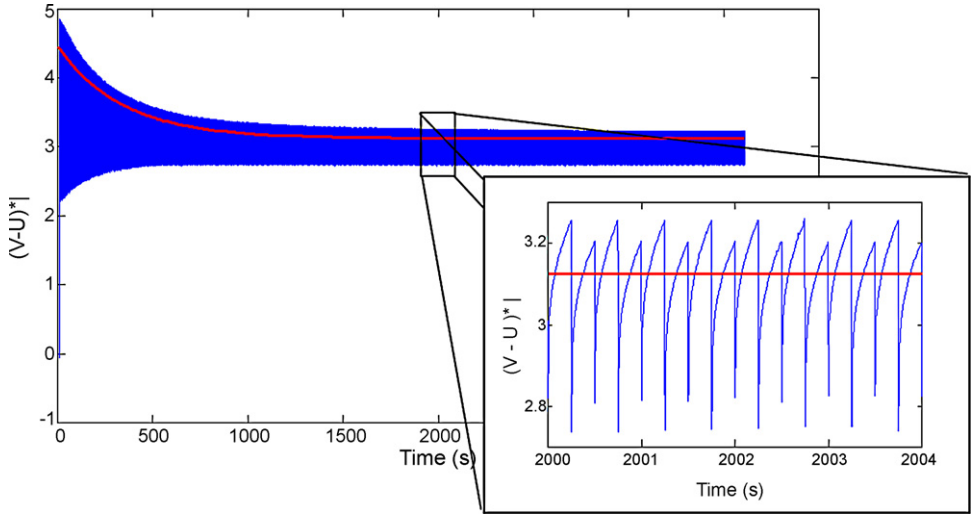

Fig. 5. Evolution of $(V - U)I$ (blue) and corresponding smoothed curve (red). (For interpretation of the references to color in this figure legend, the reader is referred to the web version of the article.

internal heat transfer resistors can be combined into a single one called R_{in} in the simplified equivalent circuit of Fig. 6b. In the same way, the external heat transfer resistors are combined, yielding an equivalent resistor R_{out}.

In order to assess the validity of the assumption of surface temperature uniformity, infrared imaging was carried out. The battery was first painted in black so as to get a well-defined emissivity, which was set to unity. Infrared photos of the battery terminals and of the lateral surface were recorded while increasing the battery temperature using current pulses as described in Section 2. Fig. 7 displays the infrared images of the lateral and the terminal surfaces at the end of the test (after an hour with pulses at ±15 A). This clearly shows that the temperature difference between the different surfaces is within 2 °C. This validates that the simplified equivalent circuit of Fig. 6b can be used to model the thermal behavior of the battery.

4. Determination of the model parameters

In this section, values for the three parameters of the model (R_{in}, R_{out}, and C_p) are extracted from the experimental data. All the parameters can be obtained from a single current-pulse experiment: R_{in} and R_{out} are determined from the thermal steady state part while the transient part allows for the determination of C_p. As explained in Section 2, several current-pulse experiments were carried out under different current magnitudes, and a set of parameter values was obtained for each experiment, with the goal of assessing the temperature influence on the parameter values.

4.1. Determination of R_{out}

Using the simplified equivalent circuit (Fig. 6b), the surface temperature is obtained by solving for the first-order differential equation

$$\frac{dT_{surf}}{dt} = \frac{T_{amb} - T_{surf}}{C_p(R_{in} + R_{out})} + \frac{\dot{Q}R_{out}}{C_p(R_{in} + R_{out})}. \quad (4)$$

When a thermal steady state is reached, the term dT_{surf}/dt goes to zero, which means that all the heat flux generated by the heat source $\dot{Q}$ flows through R_{in} and R_{out}. Eq. (4) then reads

$$R_{out} = \frac{T_{surf,\infty} - T_{amb}}{\dot{Q}_\infty}, \quad (5)$$

where the index ∞ means that the value is taken at thermal steady state (after an hour under current pulses in this study). The values of R_{out} determined from the thermal steady state data for the three experimental values of current magnitude are provided in Table 1.

Table 1
Values of R_{out}, R_{in}, R_{in}/R_{out}, and C_p determined from current-pulses experiments with different current magnitudes.

Pulse	±10 A	±15 A	±20 A
R_{out}(K W^{-1})	9.12	9.08	8.44
R_{in}(K W^{-1})	3.273	3.386	3.20
R_{in}/R_{out}	0.359	0.373	0.379
C_p(J K^{-1})	73.2	77.7	77.9

It is seen that the values of R_{out} are fairly dispersed, and a slight decrease is observed when the magnitude of the current pulses (and therefore the thermal steady state surface temperature) increases. Although this might point out a temperature-dependence of the heat transfer coefficient of the air surrounding the battery, experimental uncertainties on temperature measurements have a rather large impact on the values of R_{out}. As an example, if an ambient temperature of 23 °C is taken instead of 22 °C, a value of 8.135 K W^{-1} is obtained for R_{out}.

4.2. Determination of the ratio R_{in}/R_{out}

Because the same heat flux flows through R_{in} and R_{out}, the ratio R_{in}/R_{out} can be simply expressed in terms of the internal temperature, the surface temperature, and the ambient temperature of the air, which reads

$$\frac{R_{in}}{R_{out}} = \frac{T_{in} - T_{surf}}{T_{surf} - T_{amb}}. \quad (6)$$

Note that this relationship is valid at all times. The values of R_{in}/R_{out} determined at thermal steady state are reported in Table 1 for the three experimental values of current magnitude together with

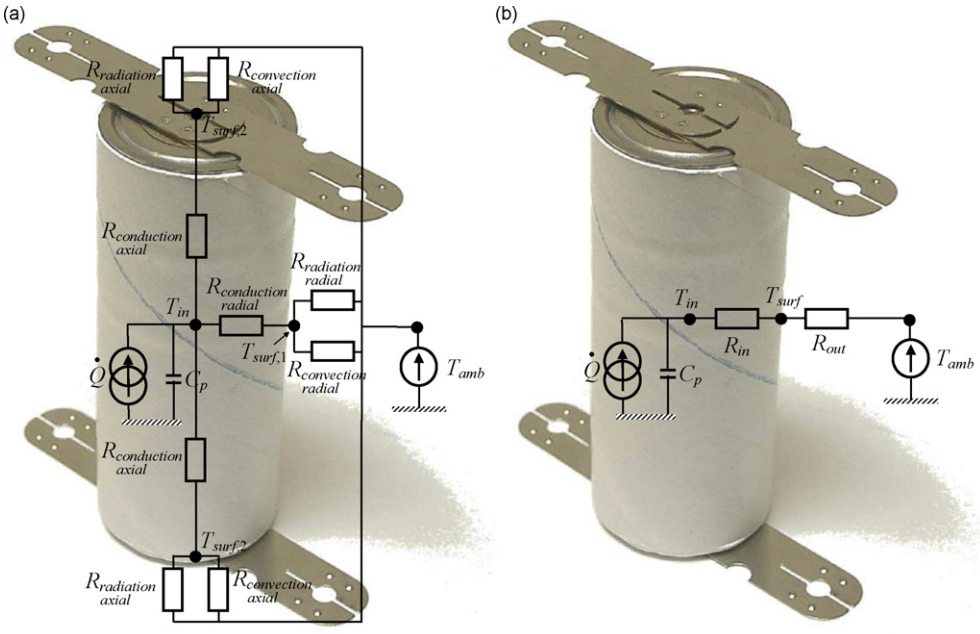

Fig. 6. Lumped models ((a) complete model and (b) simplified model).

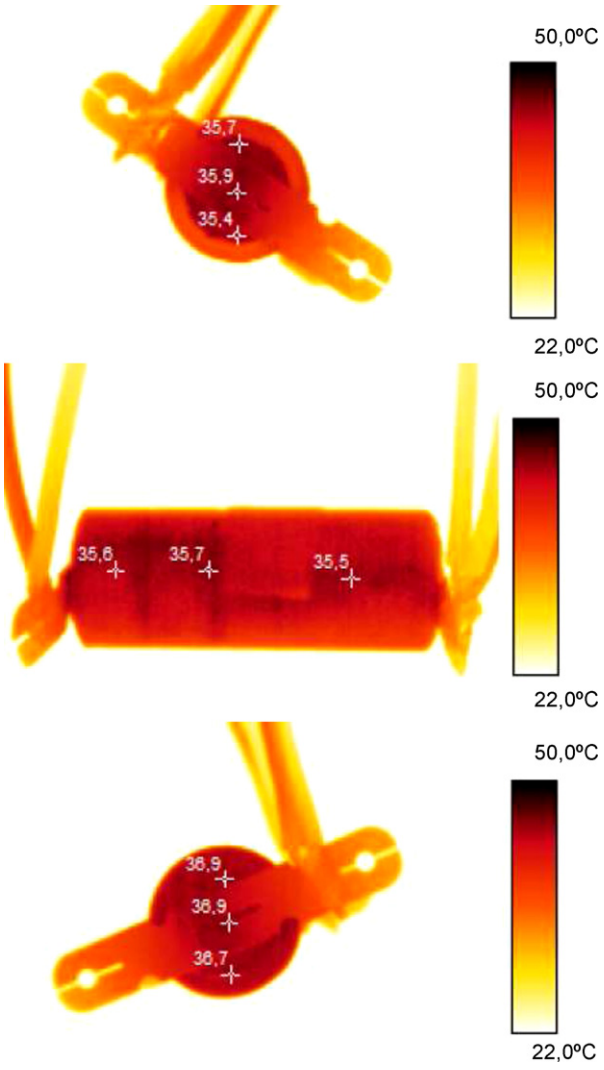

Fig. 7. From top to bottom: Infrared images of the negative terminal, lateral surface, and positive terminal of the battery after a one-hour test (±15 A).

those for R_{in}. As mentioned above for R_{out}, it is hard to get a feel on whether the slight increase of the ratio R_{in}/R_{out} with the magnitude of the current pulses is significant, since it is probably within the experimental error on temperature measurements.

4.3. Determination of C_p

Using the values of R_{in} and R_{out} determined at thermal steady state (Table 1), the heat capacity of the battery C_p can be obtained from the transient part of the experiment through an optimization routine based on least-square regression on the surface temperature as a function of time. The optimization consists in minimizing the residues between the calculated surface temperature as a function of time (using Eq. (4)) and the experimental measurements. Just like for the determination of R_{in} and R_{out}, values of C_p were refined separately for the three experimental conditions. Note that because only slight (and maybe not significant) variations of R_{in} and R_{out} were found for the three experiments, the temperature dependence of those two variables was discarded here and the values determined at thermal steady state were used to fit a transient thermal effect, during which the surface temperature varies significantly. The values of the heat capacity are presented in Table 1.

The values obtained for each experiment are fairly close to each other (6% deviation between the two extreme values of C_p). Note that the error on C_p values encompass those on R_{in} and R_{out}, and therefore can be significantly high.

5. Model validation

Using the simplified model, it is now possible to estimate the internal temperature of the battery once its surface temperature and the ambient temperature are known. This is done simply by means of the equation

$$T_{in} = T_{surf}\left(1 + \frac{R_{in}}{R_{out}}\right) - T_{amb}\frac{R_{in}}{R_{out}}. \quad (7)$$

For validation purpose, the battery was tested under various experimental conditions in order to assess the validity of the model and the values of input parameters.

5.1. 0.05 Hz current pulses at 40 °C

In a first validation, the battery was placed in a thermal chamber at 40 ° C and the thermal sequence consisted in long periods (5 or 10 min) during which either 0.05 Hz current pulses (±10 or ±20 A) or rest periods were applied to the battery.

Fig. 8 shows the estimation results of the internal temperature of the battery during this thermal sequence, for which a value of $R_{in}/R_{out} = 0.379$ was used (value for ±20 A). In that case, the difference between the estimated and measured internal temperature lies within 1.5 °C. Note, though, that similar errors are found when estimating the internal temperature using R_{in}/R_{out} values obtained from either ±10 or ±15 A current-pulse experiments.

5.2. Charge/discharge at 6 C and 24 °C

A second validation consisted in a high-rate charge/discharge of the battery at a current of 13.8 A (corresponding to 6 C). Upon reaching the upper cutoff potential on charge (3.6 V), the voltage was held at this value until the current decayed to 0.5 A. The voltage and current profiles are given in Fig. 9. During the test, the battery was simply in contact with ambient air at a temperature of 24 °C.

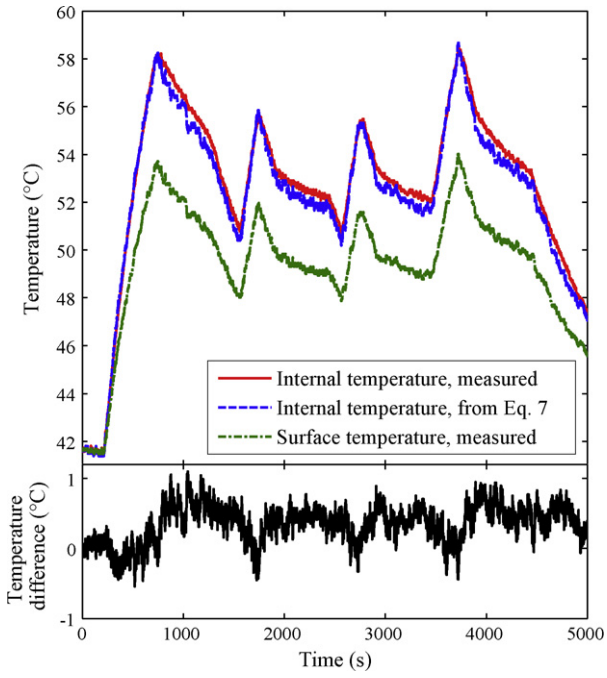

Fig. 8. Estimations of T_{in} from T_{surf} for the current-pulse experiment used for validation. R_{in}/R_{out} is set to 0.379 (value for ±20 A).

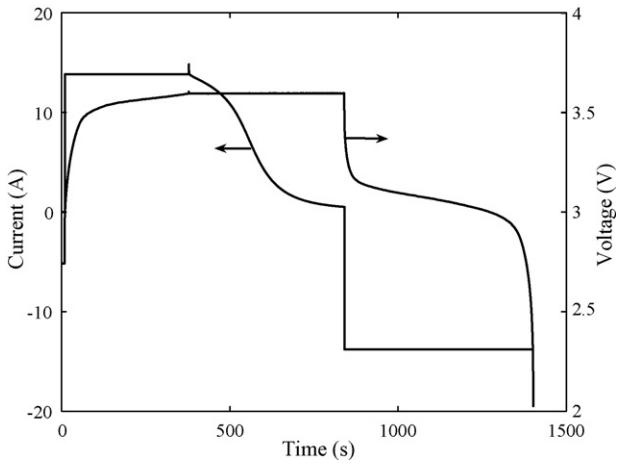

Fig. 9. Current and voltage profile during a charge/discharge of the battery at a current of 13.8 A. The constant current–constant voltage (CCCV) protocol was used on charge.

Using infrared imaging, the surface temperature was shown to be pretty uniform (not shown here).

As done above for the current-pulse profile, the internal temperature is calculated from the measured surface temperature by means of Eq. (7), using R_{in}/R_{out} values obtained from ±15 A current-pulse experiments. As seen in Fig. 10, the difference between measured and estimated internal temperature is within ca. 1.2 °C, which is satisfactory.

Finally, the internal temperature is directly estimated from current and voltage profiles, using the overall energy balance (Eq. 1), where q_n is expressed as

$$q_n = \frac{T_{in} - T_{amb}}{R_{in} + R_{out}}, \tag{8}$$

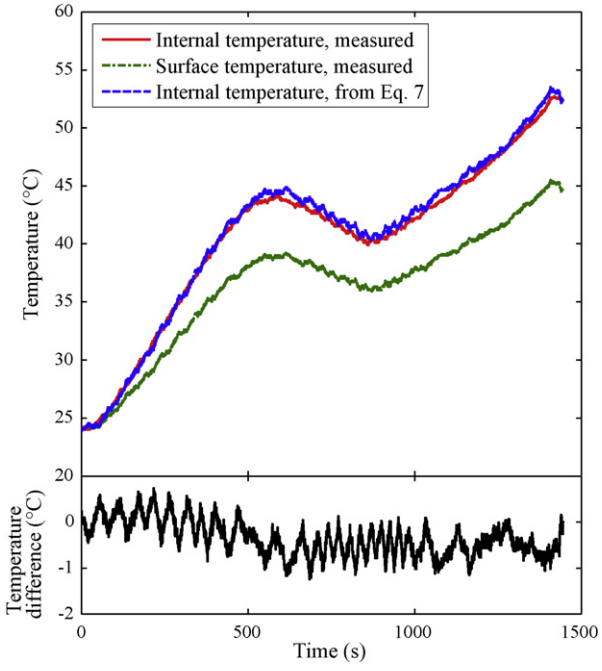

Fig. 10. Estimations of T_{in} from T_{surf} for the full charge/discharge experiment at 13.8 A. R_{in}/R_{out} is set to 0.373 (value for ±15 A).

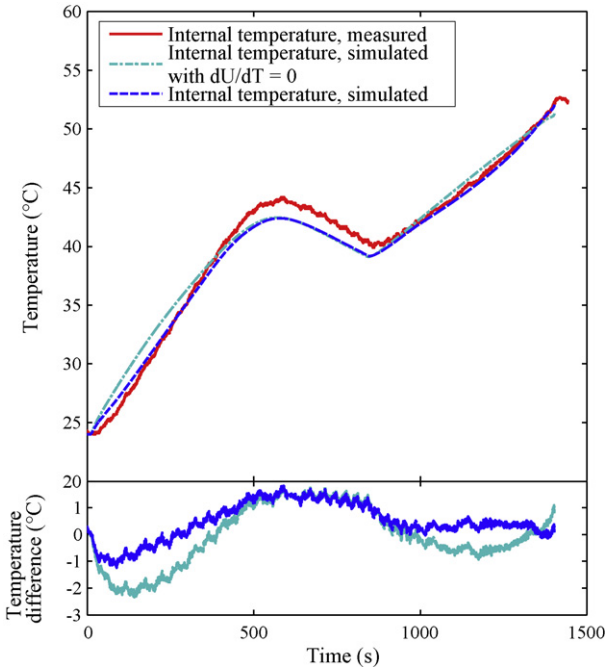

Fig. 11. Estimations of T_{in} for the full charge/discharge experiment at 13.8 A using the voltage and current. Values of model parameters obtained from current-pulses experiments at ±15 A were used.

by a rearrangement of Eq. (2) to cancel T_{surf}. Eq. (3) is used for $\dot{Q}$, with the two terms on the right side being set to zero

$$\dot{Q} = I(V - U^{\text{avg}}) + IT\frac{\partial U^{\text{avg}}}{\partial T}. \tag{9}$$

The open-circuit potential U at various temperatures and the temperature coefficient $\partial U/\partial T$ were determined experimentally as a function of the SOC (see above).

In order to solve for the internal temperature, the energy balance was solved at each time. This is a simple initial-value problem. The energy balance was discretized in time using the (first-order) Euler method with a time step of 0.1 s. The simulated internal temperature is overlaid to the experimental one in Fig. 11. There is a good agreement between the two, especially under constant current. The error is larger under constant voltage charging (maximum temperature difference of 1.8 °C), probably because of a larger error on U and $\partial U/\partial T$ near full charge (SOC ≈ 100%). As a way to assess the importance of the reversible heat source term (second term on right side of Eq. (9)), the internal temperature was determined by setting this term to zero, and is shown in Fig. 11. The temperature difference between the measured and simulated internal temperature is larger when the reversible term is neglected, especially during the charge (maximum temperature difference of 2.3 °C), and near the end of discharge. This emphasizes the importance of considering this term in the simulations when the conditions used above for current-pulse experiments (symmetric pulses having a short period) are not fulfilled.

6. Conclusion

A simple thermal model of a cylindrical $LiFePO_4$/graphite lithium-ion battery was developed. A thermocouple was inserted in the battery so as to measure the internal temperature and therefore to determine the input parameters for the model. A difference up to 10 ° C was observed between the center of the battery and the surface, which emphasizes the need for taking into account the

temperature distribution in dynamic models used in BMS. Using the model and measurements of the surface temperature by means of a surface-mounted thermocouple, the internal temperature of the battery could be determined with an error less than 1.5 °C. The estimation method of the internal temperature is very straightforward and readily implementable on a low-cost micro-controller for BMS, and could greatly improve the accuracy of the electrochemical model since input parameters are temperature-dependent. This work is a preliminary study, and the final goal is to achieve a complete thermal model of a battery pack. In order to simplify the use of the proposed method in the case of a pack, future work will focus on methods that do not require a thermocouple inserted in the battery.

Acknowledgment

The authors acknowledge the Région Picardie for the financial support.

References

[1] H.J. Bergveld, W.S. Kruijt, P.H.L. Notten, Battery Management Systems, Design by Modelling, vol. 1, Kluwer Academic Publishers, 2002.
[2] P.M. Gomadam, R.E. White, J.W. Weidner, Journal of the Electrochemical Society 150 (10) (2003) A1339–A1345.
[3] S. Al-Hallaj, H. Maleki, J.S. Hong, J.R. Selman, Journal of Power Sources 83 (1–2) (1999) 1–8.
[4] K. Smith, C.Y. Wang, Journal of Power Sources 160 (1) (2006) 662–673.
[5] S.A. Khateeb, S. Amiruddin, M. Farid, J.R. Selman, S. Al-Hallaj, Journal of Power Sources 142 (1–2) (2005) 345–353.
[6] G.H. Kim, A. Pesaran, R. Spotnitz, Journal of Power Sources 170 (2) (2007) 476–489.
[7] E. Barsoukov, J.H. Jang, H. Lee, Journal of Power Sources 109 (2) (2002) 313–320.
[8] W.M. Deen, Analysis of Transport Phenomena, Oxford University Press, 1998.
[9] K.E. Thomas, J. Newman, Journal of the Electrochemical Society 150 (2) (2003) A176–A192.
[10] K.E. Thomas, Ph.D. Thesis, University of California, Berkeley, 2002.
[11] K.E. Thomas, C. Bogatu, J. Newman, Journal of the Electrochemical Society 148 (6) (2001) A570–A575.
[12] Y. Reynier, R. Yazami, B. Fultz, Journal of Power Sources 119–121 (2003) 850–855.